Journal of Hazardous Materials 197 (2011) 294–303

Contents lists available at SciVerse ScienceDirect

Journal of Hazardous Materials

journal homepage: www.elsevier.com/locate/jhazmat

Interactions of NO_2 at ambient temperature with cerium–zirconium mixed oxides supported on SBA-15

Benoit Levasseur[a], Amani M. Ebrahim[a], Jacob Burress[b], Teresa J. Bandosz[a,*]

[a] The City College of New York and The Graduate School of CUNY 160 Convent Ave, New York, NY 10031, USA
[b] NIST Center for Neutron Research, National Institute of Standards and Technology 100 Bureau Drive, Gaithersburg, MD 20899, USA

ARTICLE INFO

Article history:
Received 4 August 2011
Received in revised form
20 September 2011
Accepted 22 September 2011
Available online 29 September 2011

Keywords:
Ambient conditions
Cerium
NO_x adsorption
SBA-15
Zirconium

ABSTRACT

New silica-based composites were obtained using a slow precipitation of mixed oxide $Ce_{1-x}Zr_xO_2$ on the surface of mesoporous silica, SBA-15. The samples were tested as NO_2 adsorbents in dynamic conditions at room temperature. The surface of the initial and exhausted materials was characterized using N_2 sorption, XRD, TEM, potentiometric titration, and thermal analysis before and after exposure to NO_2. In comparison with unsupported $Ce_{1-x}Zr_xO_2$ mixed oxides, a significant increase in the NO_2 adsorption capacity was observed. This is due to the high dispersion of active oxide phase on the surface of SBA-15. A linear trend was found between the NO_2 adsorption capacity and the amount of $Zr(OH)_4$ added to the structure. Introduction of Zr^{4+} cations to ceria contributes to an increase in the amount of Ce^{3+}, which is the active center for the NO_2 adsorption, and to an increase in the density of –OH groups. These groups are found to be involved in the retention of both NO_2 and NO on the surface. After exposure to NO_2, an acidification of the surface caused by the oxidation of the cerium as well as the formation of nitrite and nitrates took place. The structure of the composites appears not to be affected by reactive adsorption of NO_2.

1. Introduction

Air pollution originated from nitrogen oxides (NO_x) causes a great damage to the environment. NO_2 and NO molecules are byproducts of industrial manufacturing processes, mobile exhaust, fossil fuel combustion and power generating sources. They contribute to the formation of photochemical smog and acid rain. Therefore, due to a constant increase of energy consumption the removal of nitrogen oxides has become an important target in environmental catalysis. Additionally, efficient adsorbents, being able to retain large quantity of NO_x at ambient conditions, are in need for modern respirator cartridges and air filters.

Selective catalytic reduction by hydrocarbons (SCR) [1–3] and NO_x storage and reduction catalysis (NSR) [4,5] are among the most studied methods causing a decrease of nitrogen oxide concentrations in air. Even though these methods use very promising cerium-based catalysts, they still suffer from limitations such as release of unreacted ammonia and hydrocarbons and the requirement of high temperatures [6]. The redox cycle between Ce^{4+} and Ce^{3+} appears to be an important parameter governing the adsorption of NO_x in a fixed bed [7–9]. The reduction of Ce^{4+} cation is associated with the formation of oxygen vacancies located right next to the Ce^{3+} cation. These oxygen vacancies were found to be highly reactive with NO_2, leading to the formation of nitrite and nitrate species by electron transfer reaction [7,8]. Knowing the importance of this system, the control of the Ce^{3+}/Ce^{4+} ratio may lead to a higher reactivity of ceria-based materials towards the NO_x separation process. It is known that the reducibility of Ce^{4+} into Ce^{3+} can be enhanced by addition of Zr^{4+} cation as a doping agent [10–13]. Several studies indicate that the energy required to achieve the reduction of Ce^{3+} into Ce^{4+} is decreased by increasing the content of Zr in $Ce_{1-x}Zr_xO_2$ mixed oxides. [10,11]. The addition of Zr^{4+} to the ceria structure, not only influences the redox cycle Ce^{3+}/Ce^{4+}, but also increases the stability, the oxygen storage capacity as well as the catalytic activity of the ceria at lower temperatures [14–16].

Since the beginning of the 90s the synthesis of silica mesostructured materials [17] has been extensively studied. Due to the wide range of pore size (ranging from 2 to 50 nm) these structures overcome the diffusion limitations of microporous solids such as zeolites. Therefore these silica-based materials, including MCM-41 and SBA-15, with high surface areas and tunable pore sizes are excellent candidates for modifications by the introduction of organic groups [18,19], metals [20–22] or oxides [23–25]. The thick wall of the SBA-15, in comparison with MCM-41, makes this structure more thermally and hydrothermally stable which is an

* Corresponding author. Tel.: +1 212 650 6017; fax: +1 212 650 6107.
E-mail address: tbandosz@ccny.cuny.edu (T.J. Bandosz).

0304-3894/$ – see front matter © 2011 Elsevier B.V. All rights reserved.
doi:10.1016/j.jhazmat.2011.09.087

important feature when this material is used as a catalyst support [26]. Even though the main applications of silica are in separation science and catalysis, the literature regarding its application for NO_2 adsorption is rather scarce to our best knowledge. In some cases the SBA-15 composite is reported as a NO_2 sensor when used as a support to disperse WO_3 [27] or as a template to prepare mesoporous ZnO [28].

Considering the above, as well as our promising results on NO_2 adsorption at room temperature on $Ce_{1-x}Zr_xO_2$ mixed oxides [29], the aim of this study is to take advantage of the large surface area and pore volume of SBA-15 and use this material as a support for an active mixed oxide phase. The synthesized composite materials are tested for NO_2 adsorption at room temperature and extensively characterized in order to derive a mechanism and to identify the surface feature important for the retention process at ambient conditions.

2. Experimental

2.1. Materials

SBA-15 mesoporous silica was synthesized following the procedure introduced in Ref. [30]. 2.0 g of poly(ethylene glycol)-block-poly(propylene glycol)-block-poly(ethylene glycol) (also known as P123) was dissolved in 60 mL of 2.0 M HCl at room temperature and 8.8 g of KCl was added to the solution. Then 4.2 g of tetraethyl orthosilicate (TEOS) was added under vigorous stirring. The final reactant molar composition was 0.02 P123/6 KCl/6 HCl/166 H_2O/1 TEOS. After stirring at room temperature for a day, the mixture was transferred into an autoclave and heated at 100 °C for 24 h. The product was, then, collected by filtration and washed with both ethanol and water (to remove unreacted P123 and KCl) and dried. The as-made powder was calcined at 550 °C for 6 h to remove the organic template.

Appropriate amounts of cerium and zirconium chlorides (0.05 M) were slowly added drop by drop with a rate of 0.6 mL/min to a suspension consisting of a mixture of NaOH (0.05 M) and 0.7 g of SBA-15. It was done to precipitate $Ce_{1-x}Zr_xO_2$ with $x = 0$, 20, 40, 60, 80 and 100 on the surface of SBA-15. The loading of mixed oxides on silica surface was 25 wt.%. Single cerium oxide or zirconium hydroxide was also precipitated on the surface of SBA-15 using cerium or zirconium chloride (0.05 M).

After completion of the precipitation process the product was collected by filtration and washed with water to remove Cl^- ions and dried. The powder was used in a breakthrough test without any heat treatment. These materials are referred to as Si–CZ*x* with $x = 0$, 20, 40, 60, 80 and 100, where Si–CZ0 and Si–CZ100 refers respectively to pure ceria and to pure zirconium hydroxide both dispersed on SBA-15. The numbers correspond to the molar percentage of $Zr(OH)_4$ in the CeO_2 structure.

2.2. Methods

2.2.1. NO_2 breakthrough capacity

The NO_2 breakthrough capacities were measured in a laboratory-scale, fixed-bed reactor system, at room temperature and in dynamic conditions. In a typical test, 1000 ppm NO_2 in nitrogen went through a fixed bed of an adsorbent with a total inlet flow rate of 225 mL/min. The adsorbent was packed into a glass column (length 370 mm, internal diameter 9 mm). About 2 cm^3 of glass beads well mixed with adsorbent are required to obtain a homogeneous bed and to avoid pressure drop. The concentrations of NO_2 and NO in the outlet gas were measured using an electrochemical sensor (RAE Systems, MultiRAE Plus PGM-50/5P)[1]. The adsorption capacity of each adsorbent was calculated in mg/g of adsorbent by integration of the area above the breakthrough curve. The tests were conducted until the concentrations of NO_2 and NO reached the electrochemical sensors' upper limit values of 20 ppm and 200 ppm, respectively. After the breakthrough tests, all samples were exposed to a flow of carrier air (180 mL/min) to desorb weakly adsorbed NO_x and thus to evaluate the strength of NO_2 retention. The suffix – ED is added to the names of the samples after exposure to NO_2.

2.2.2. Surface pH

The samples were first dried and then 0.4 g was added to 20 mL of distilled water and stirred overnight. The pH of the suspension was then measured.

2.2.3. XRD

Low angle and high angle X-ray diffraction patterns (PXRD) were respectively obtained on a Rigaku Ultima III powder diffractometer and a Philips X'Pert X-ray diffractometer using CuK_α radiation with a routine power of 1600 W (40 kV, 40 mA).

2.2.4. TEM

Transmission electron microscopy (TEM) was performed on a Zeiss EM 902 instrument. The microscope has a line resolution of 0.34 nm and a point resolution of 0.5 nm and operates in normal diffraction, and low dose modes at 50 or 80 kV. Analyses were performed on dry films obtained after the samples were re-suspended in ethanol.

2.2.5. Adsorption of nitrogen

Nitrogen isotherms were measured at −196 °C using an ASAP 2010 or ASAP 2050 (Micromeritics). Prior to each measurement, initial and exhausted samples were outgassed at 120 °C. The surface area, S_{BET}, the total pore volume, V_t, the micropore volume, V_{mic} (Dubinin–Radushkevitch method [31]), and the mesopore volume, V_{mes}, were obtained from the isotherms. Pore size distributions were calculated using density functional theory [32].

2.2.6. Potentiometric titration

Potentiometric titration measurements were performed with a DMS Titrino 716 automatic titrator (Metrohm). The instrument was set at the mode when the equilibrium pH was collected. Subsamples of the materials studied of about 0.100 g in 50 mL 0.01 M $NaNO_3$ were placed in a container thermostatted at 298 K and equilibrated overnight with the electrolyte solution. To eliminate the influence of atmospheric CO_2, the suspension was continuously saturated with N_2. The suspension was stirred throughout the measurements. Volumetric standard NaOH (0.1 M) was used as the titrant. The experiments were done in the pH range of 3–10. Each sample was titrated with base after acidifying the sample suspension. The experimental data was transformed into a proton binding curves, *Q*, representing the total amount of protonated sites [33].

2.2.7. Thermal analysis

Thermogravimetric (TG) curves and their derivatives (DTG) were obtained using a TA Instruments thermal analyzer. The samples (initial and exhausted) were previously dried in oven at 100 °C to remove the adsorbed moisture and then heated up to 1000 °C, with a heating rate 10 °C/min under a nitrogen flow of 100 mL/min.

[1] Certain trade names and company products are mentioned in this paper to adequately specify the experimental procedure and equipment used. In no case does this imply recommendation or endorsement by NIST, nor does it imply that the products are necessarily the best available for this purpose.

Table 1
NO_2 breakthrough capacities and pH values before and after the exposure to NO_2 for the SBA-15 and the composites.

Samples	pH ini	NO_2 capacity [mg/g]	NO released[%]	pH fin
SBA-15	6.87	21	12	6.52
Si–CZ0	6.15	37	15	5.77
Si–CZ20	6.25	127	8	4.72
Si–CZ40	7.58	194	7	4.99
Si–CZ60	7.70	240	7	4.83
Si–CZ80	8.18	318	6	4.63
Si–CZ100	8.28	54	14	7.85

3. Results and discussion

The NO_2 breakthrough curves on single and mixed oxide, $Ce_{1-x}Zr_xO_2$, dispersed on SBA-15 mesoporous silica are shown on Fig. 1. The curves measured on SBA-15 and the single oxides Si–CZ0 and Si–CZ100 appear to be steeper than the ones obtained for the mixed oxides, suggesting a difference in the adsorption mechanism. Regardless, the composition of the mixed oxides dispersed on SBA-15, their retention times are always higher than for the single oxides and SBA-15. The NO_2 retention time on Si–CZ materials (excluding CZ0 and CZ100) increases with an increase in the amount of $Zr(OH)_4$ in the structure. This suggests an important role of Zr^{4+} cations and/or –OH groups in NO_2 adsorption [10,11,29].

The NO_2 breakthrough capacities of each material were calculated and they are collected in Table 1. They range between 21 mg_{NO_2}/g on SBA-15 and 318 mg_{NO_2}/g on Si–CZ80. The measured over 30 wt.% of NO_2 adsorbed at room temperature on the latter materials is much higher that those reported so far on modified activated carbons [34–37]. A following increasing order in capacities is observed: SBA-15 < Si–CZ0 < Si–CZ100 < Si–CZ20 < Si–CZ40 < Si–CZ60 < Si–CZ80.

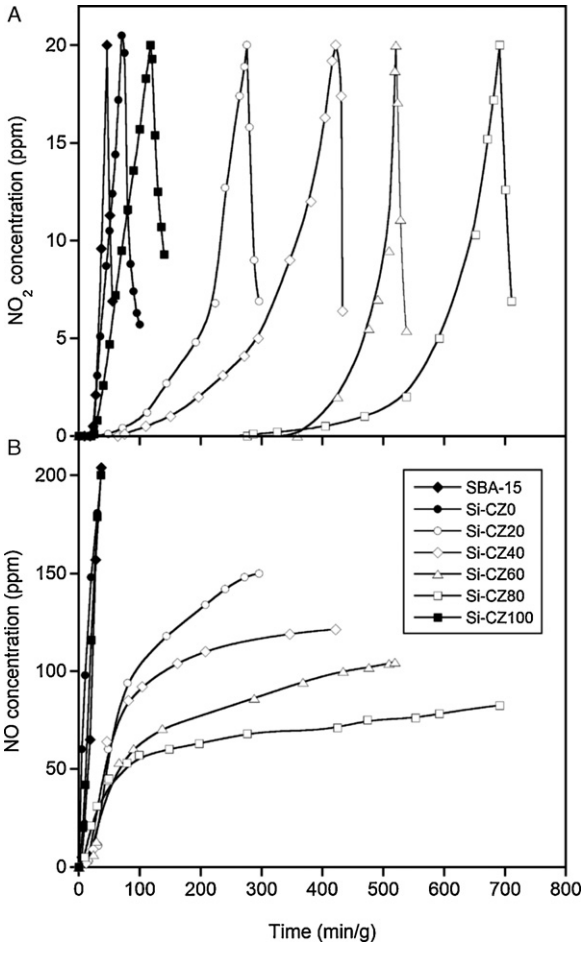

Fig. 1. NO_2 breakthrough curves (A) and NO concentration curves (B) on SBA-15 and $Ce_{1-x}Zr_xO_2$ in SBA-15 materials.

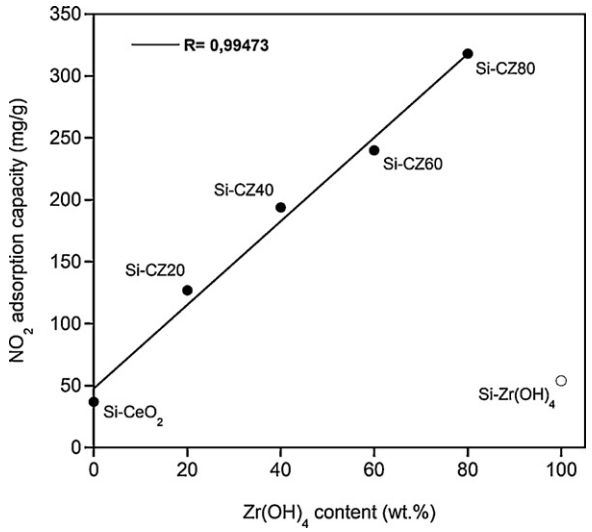

Fig. 2. Correlation between the NO_2 adsorption capacity and the content of $Zr(OH)_4$.

Fig. 2 shows the linear dependence between the NO_2 adsorption capacity and the amount of $Zr(OH)_4$ present on SBA-15. Interestingly, the capacity of Si–CZ0 follows the trend but that of Si–CZ100 does not. This suggests that even though cerium alone provides important adsorption sites for NO_2, an increase in the $Zr(OH)_4$ content leads to an enhancement in the cerium reactivity. Knowing that the Ce^{3+} is the reactive species in NO_2 adsorption process [29], we link the observed increase in the capacity to the reduction of Ce^{4+} into Ce^{3+}, which is more pronounced with an increase of the content in Zr^{4+} cations according to the Eq. (1). An addition of Zr^{4+} to the CeO_2 structure is known to promote the Ce^{4+}/Ce^{3+} redox cycle [11].

$$CeO_2 + Zr^{4+} \rightarrow Ce_{1-y}Zr_yO_2 \rightarrow Ce_{1-y}Zr_yO_{2-x} + 1/2xO_2(g) \quad (1)$$

Fig. 3 shows the comparison of the NO_2 adsorption capacities obtained on the $Ce_{1-y}Zr_yO_2$ materials alone and dispersed on mesoporous silica. The former results were reported and discussed in

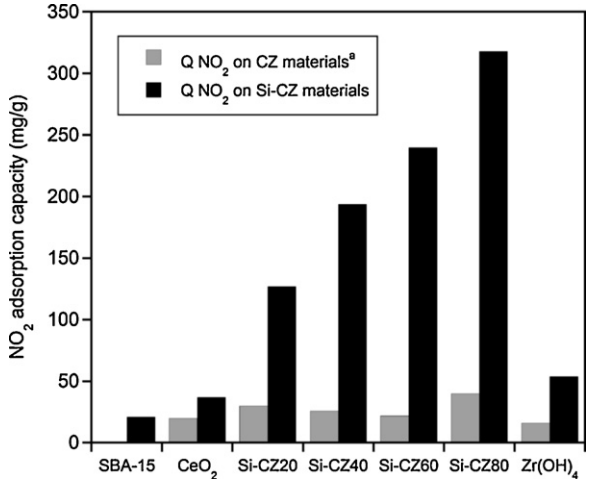

Fig. 3. Comparison of NO_2 adsorption capacity of CZ mixed oxides [29] and Si–CZ composites.

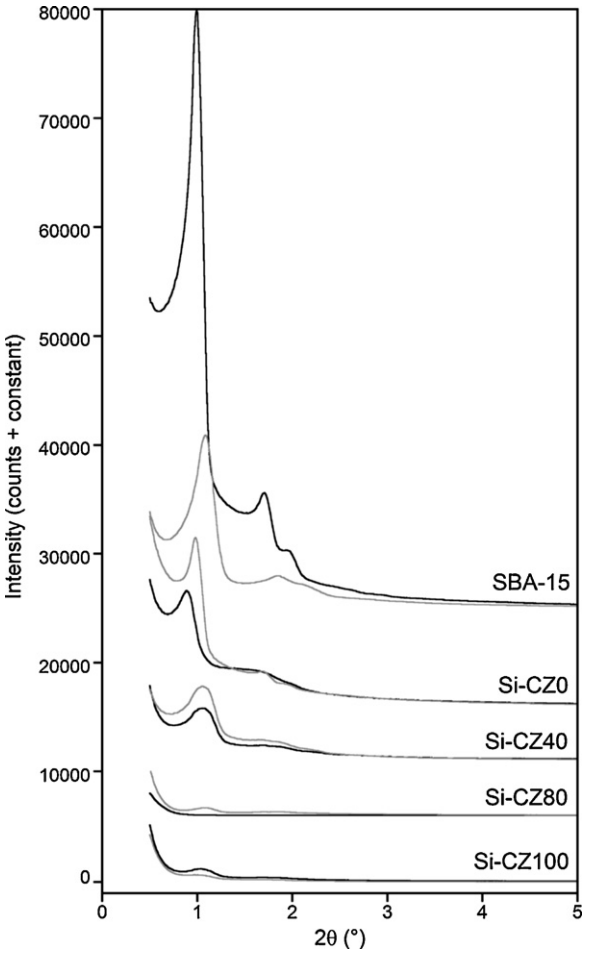

Fig. 4. Small angle X-Ray diffraction patterns of Si–CZ composites before and after exposure to NO_2.

Ref. [29]. It is clear that the deposition of mixed oxides on SBA-15 increases up to more than 10 times the amount of NO_2 adsorbed. The positive effect is also observed for the single oxides. A plausible reason for this increase is a high dispersion of oxides on the surface and thus in n accessibility of the reactive sites. To support this hypothesis the porous structure and surface chemistry of our materials have to be investigated in detail.

Another important aspect of the NO_2 removal process is the retention of NO potentially formed in surface reactions [29]. The measured concentration profiles of NO detected during the NO_2 breakthrough tests are presented in Fig. 1. The calculated percentage of NO released during the experiments is listed in Table 1. As for the NO_2 breakthrough curves, a poor retention of NO was observed on SBA-15 and on the single oxides. The released NO reached 12% on SBA-15 and 14% and 15% on Si–CZ0 and Si–CZ100, respectively. On the other hand on the mixed oxide composites only between 8% and 6% of adsorbed NO_2 was released as NO. These amounts are very small compared to those measured on other adsorbents such as activated carbons [38] or MOFs [39]. Moreover, a linear decrease is found between the percentage NO released and an increase in the zirconium content and thus in the amount of –OH groups associated with zirconium hydroxide [40]. Thus, as observed previously [29], Ce^{3+} cations and/or –OH groups of our materials are involved in the NO retention mechanism.

XRD patterns measured at small angles for selected materials before and after exposure to NO_2 are shown in Fig. 4. Before exposure to NO_2, the SBA-15 shows well-resolved diffraction peaks ascribed to the (1 0 0), (1 1 0) and (2 0 0) reflections. These peaks suggest a *p6mm* symmetry characteristic of a 2D-hexagonal network of pores [30]. After co-precipitation of mixed oxides the intensity of these peaks decreased, which indicates a modification in the structure order. The precipitation of mixed oxides takes place in the silica pores. This is supported by an observed shift in the position of these peaks indicating a change in the average pores size. This decrease in the degree of order is most pronounced for Si–CZ100 and Si–CZ80. They are expected to have the highest density of –OH groups originating from zirconium hydroxide. A slight dissolution of the silica in NaOH during the precipitation of cerium and zirconium could also contribute to the observed change in the materials' order. Interestingly, after NO_2 exposure a decrease in the intensity of the diffraction peaks is only found for SBA-15 ED. By contrast, on the single and mixed oxides dispersed on SBA-15 those peaks are more defined. The peaks representing the reflections (1 1 0) and (2 0 0) can even be distinguished for Si–CZ0 ED and Si–CZ40 ED. The results suggest that the SBA-15 structure of the composites is affected by the reactive adsorption of NO_2. On Si–CZ80 ED even an increase in the intensity of the main diffraction peak can be observed.

These changes in the structure of the materials are also visible on TEM images shown in Fig. 5. The highly ordered SBA-15 structure is seen in Fig. 5A whereas Si–CZ20 exhibits a slightly disordered pores network (Fig. 5B). Changes seen on the images of SBA-15 ED suggest that the adsorption of NO_2 on the mesoporous silica is a reactive process and lead to a small disorganization of the 2D-hexagonal network (Fig. 5C). Moreover, in the case of Si–CZ20 exposed to NO_2, the edge of the particles appears to be more organized than on the same materials just after precipitation and before the exposure to NO_2 (Fig. 5D vs. Fig. 5B).

XRD patterns recorded at higher angles (Fig. 6), in the range of 2θ between 5° and 70°, confirm that the single and mixed oxides are precipitated inside the porous network. No diffraction peaks attributed to cerium oxides can be distinguished for Si–CZ0 or Si–CZ40. It has to be taken into account that zirconium hydroxide is an amorphous structure [40] and consequently no specific diffraction peaks are found for Si–CZ80 and Si–CZ100. After exposure to NO_2, the specific diffraction peaks of cerium oxide are now visible on Si–CZ0 and Si–CZ20 indicating that ceria is partially separated from the silica matrix. Thus the destruction of the mesoporous silica during the NO_2 adsorption process takes place. In the case of Si–CZ100 and Si–CZ80 no real differences are noticed due to the amorphous nature of the zirconium hydroxide.

The parameters of the porous structure were calculated from nitrogen adsorption isotherms (Figs. 7 and 8). The isotherms obtained on the fresh materials show a large hysteresis, especially for SBA-15, which is typical of mesoporous materials (type IV isotherms). However a flattening of the hysteresis is observed after the precipitation procedure (on single and mixed oxides composites) and after exposure to NO_2, indicating a change in the volume of the pores. Indeed, a decrease of about 20% in the volume of pores is found after precipitation of the oxides in the SBA-15 structure on each material. It is interesting that the volume of micropores remains stable after precipitation. Regarding the changes in the specific surface area, two different trends are visible. On one hand, single oxides show a decrease from 422 m^2/g on SBA-15 to 357 m^2/g and 401 m^2/g on Si–CZ0 and Si–CZ100, respectively is observed (Table 2). On the other hand, for mixed oxides and SBA-15 composites, the specific surface area was found to be about 6% higher than that of SBA-15. The higher specific surface areas of mixed oxides in comparison with singles oxides have already been noticed in our previous work [29]. It was linked to the change in the structure from cubic to tetragonal due to the insertion of $Zr^{(4+)}$ cation in the fluorite structure of ceria [29]. SBA 15 and Si–CZ0 show almost homogeneous pore structures with predominant pore sizes of 100 Å and 96 Å, respectively. On the other hand, the bimodal distributions

Table 2
The parameters of porous structure before and after exposure to NO_2 for the SBA-15 and the composites.

Sample	S_{BET}[m^2/g]	V_{mic}[cm^3/g]	V_{tot}[cm^3/g]	V_{mic}/V_{tot}[%]	Dp[Å]
SBA-15	422	0.158	1.057	15	100
SBA-15 ED	352	0.137	0.673	20	76
Si–CZ0	357	0.158	0.661	24	96
Si–CZ0 ED	298	0.106	0.633	17	95
Si–CZ20	453	0.167	0.884	19	78
Si–CZ20 ED	372	0.147	0.773	19	81
Si–CZ40	443	0.159	0.759	21	69
Si–CZ40 ED	396	0.143	0.722	20	70
Si–CZ60	439	0.160	0.757	21	69
Si–CZ60 ED	379	0.136	0.711	19	76
Si–CZ80	458	0.168	0.799	21	69
Si–CZ80 ED	357	0.134	0.683	20	76
Si–CZ100	401	0.162	0.884	18	80
Si–CZ100 ED	385	0.147	0.790	19	79

are found for other composites with maxima at 100 Å and 70 Å. An increase in $Zr(OH)_4$ content leads to the formation of the pores with sizes of about 70 Å. We link that decrease in the size of the pores to an increase in the number of the –OH groups existing inside the pores as a consequence of incorporation of zirconium hydroxide to the structure of ceria.

After exposure to NO_2, a decrease in the specific surface area and volume of pores is found for each material. Moreover, the structure of the SBA-15 ED is strongly modified since a double hysteresis is visible on the isotherm and consequently a bimodal pore size distribution is revealed (Figs. 7 and 8). These strong modifications of the structure lead to a 17% decrease in the specific surface area and about 37% decrease in the volume of pores. Such difference after adsorption of NO_2 suggests that silanol groups are the active centers for NO_2 retention. On the composite materials the pore size distributions changed only slightly after NO_2 adsorption. Even though the biggest change in the porosity was found for Si–CZ80 (22% decrease in S_{BET} and 15% decrease in the volume of pores), which is also the best NO_2 adsorbent, no clear trend can be established between the loss of porosity and the NO_2 adsorption capacity. These slight changes in the specific surface area and volume of pores observed on composites are consistent with the results of the XRD analysis after exposure to NO_2, where CeO_2 diffraction peaks were revealed, suggesting a decrease of the crystallinity of the mesoporous structure.

The changes in porosity discussed above cannot fully explain the reactivity of our materials towards NO_2. To further analyze the mechanism of reactive NO_2 adsorption the surface chemistry has to be investigated. Proton binding curves for each material before and after exposure to NO_2 are shown in Fig. 9. Since the positive Q represents a proton uptake (basic surface) and negative proton release (acidic surface) the changes observed clearly indicate that the surface became much more acidic after exposure to NO_2. This acidification of the materials is, in addition, in agreement with the

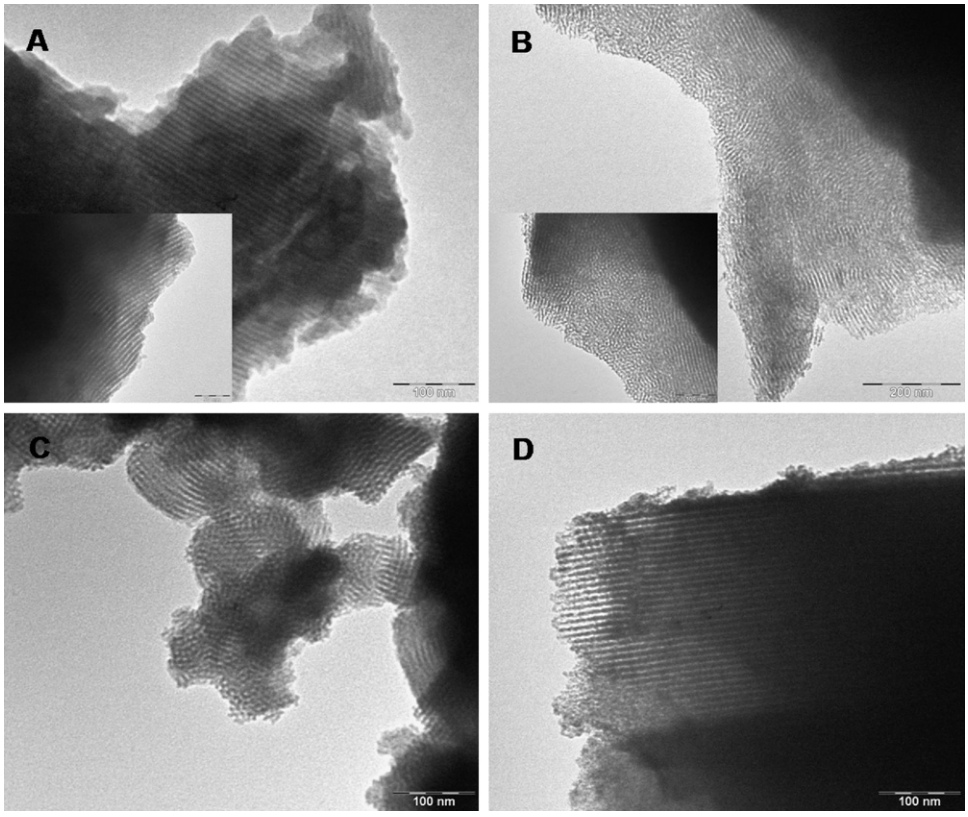

Fig. 5. TEM images of SBA-15 (A), Si–CZ20 (B), SBA-15 ED (C) and Si–CZ20 ED (D).

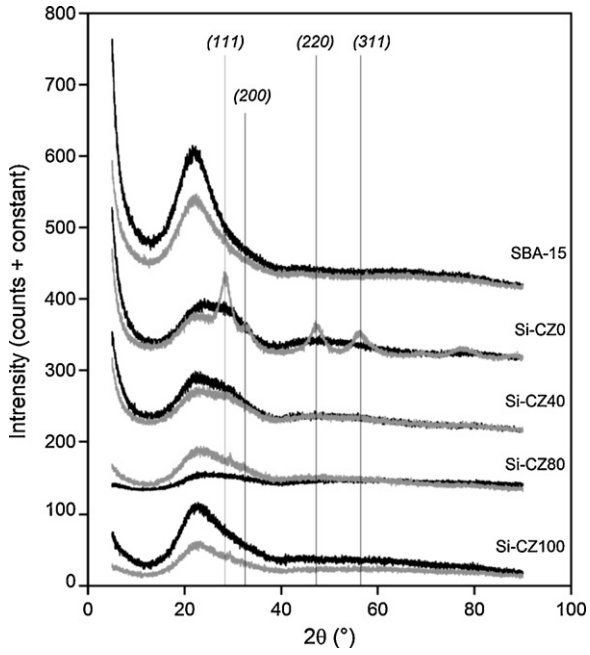

Fig. 6. X-Ray diffraction patterns of Si–CZ composites before (black) and after (grey) exposure to NO_2.

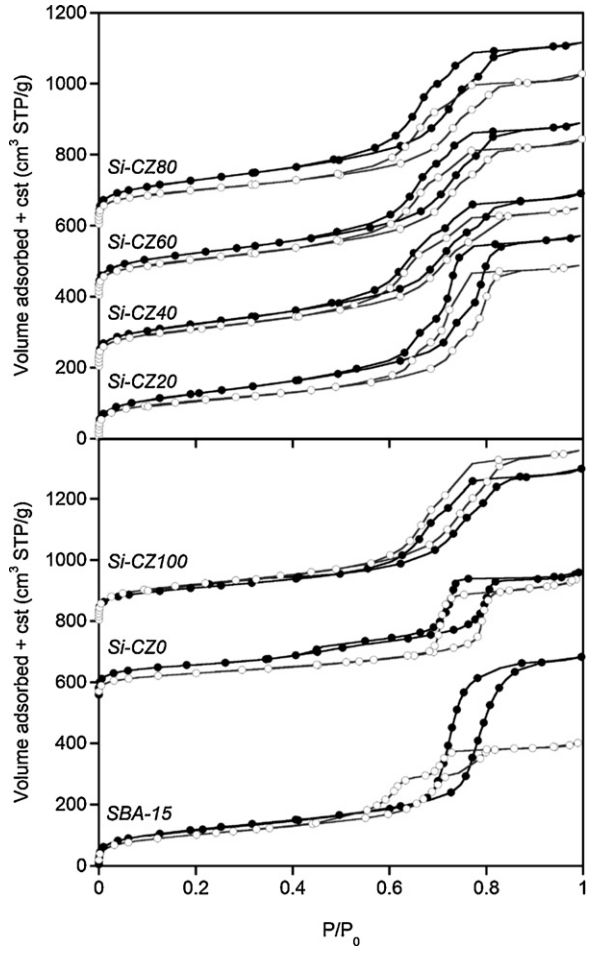

Fig. 7. Nitrogen adsorption isotherms on SBA-15 and Si–CZ composites before (black) and after (grey) exposure to NO_2.

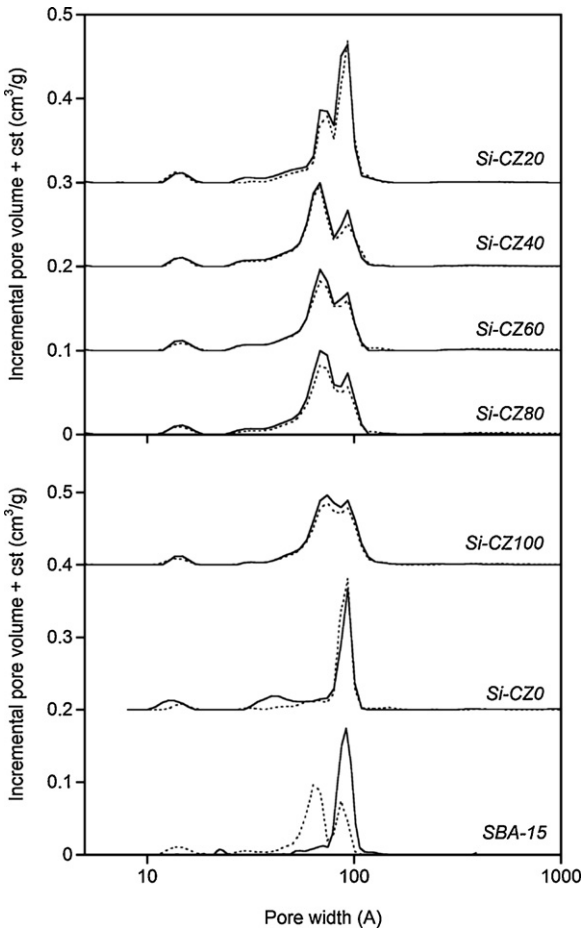

Fig. 8. Pore size distribution of SBA-15 and Si–CZ composites before (solid) and after (dotted) exposure to NO_2.

pH values measured before and after adsorption tests collected in Table 1. A shift to lower pH is also noticed for pH of zero charge ($Q = 0$ mmol/g) for each material after adsorption of NO_2. Oxidation of the surface is usually related with an acidification of the adsorbent [41,42] and it was already observed on ceria–zirconia mixed oxides [29]. This suggests that the reduced cerium in the structure, due to the insertion of $Zr^{(4+)}$ cations (Eq. (1)), is oxidized during the exposure to NO_2. Moreover the acidification is apparently correlated with the NO_2 adsorption capacity since the bigger change in the acidity of the surface is found on Si–CZ80 and Si–CZ60, which are the two best adsorbents. The pH_{pzc} of those materials is 8.7 and 7.9, respectively and it decreases to about 4.5 for both composites after exposure to NO_2. On the other hand, on single oxide/hydroxide composites and on SBA-15 alone whose NO_2 adsorption capacities are smaller, the shift of pH_{pzc} after exposure to NO_2 is much smaller (about 1–1.5 pH unit). Finally, it is interesting to note some changes in the surface chemistry of SBA-15 alone indicating that the NO_2 adsorbed during the test is not only retained via a physical adsorption mechanism. As suggested above, the silanol groups may be involved in the retention of NO_2 since the surface of SBA-15 ED became acidified/oxidized.

pK_a distributions of oxygen containing groups present on the surface of the materials studied are shown in Fig. 10. For SBA-15, four peaks are found pK_a at about 6.5, 7.8, 9 and 10.5. The first pK_a is attributed to the deprotonation of Si–OH [43] whereas the peaks at pK_a 7.8 and 9 are respectively ascribed to the first step of deprotonation of $Si(-OH)_3$ [44] and $Si(-OH)_2$ [45]. Regarding the last peak at pK_a 10.5, it is believed that it is composed by the contribution of the second and the third step of deprotonation of $Si(-OH)_3$ and

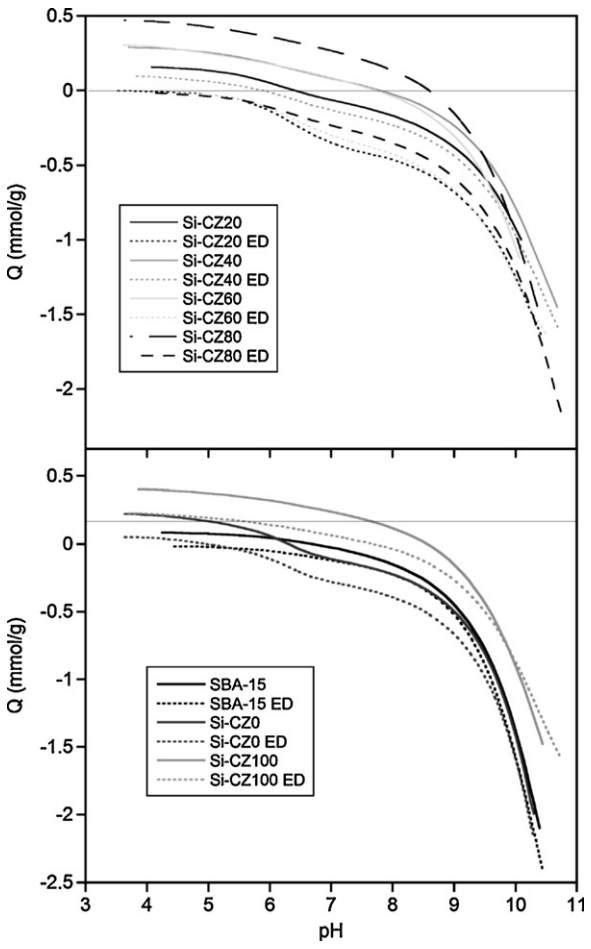

Fig. 9. Proton binding curves of Si–CZ composites before and after exposure to NO_2.

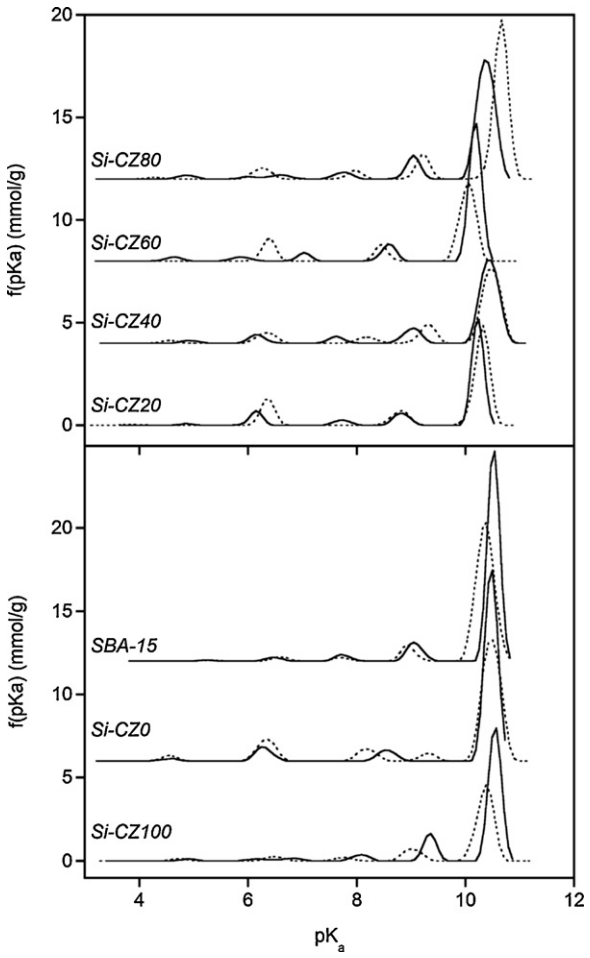

Fig. 10. pK_a distribution of SBA-15 and Si–CZ composites before and after exposure to NO_2.

$Si(–OH)_2$ as well as the deprotonation of $Si(OH)_4$ species [44]. In the case of Si–CZ100 even though the same peaks are found at similar pK_a, at the species with pK_a about 9 and 10.5 may also correspond to terminal weakly acidic Zr–OH groups [46]. On the surface of Si–CZ0, besides the peaks representing acidic groups of silica a small peak around 6.5 appears. It is assigned to the pK_a of Ce^{4+} cation [29,47]. For the mixed oxide composites, a new peak at pK_a close to 7 also represents Ce^{4+} [29]. Its similar pK_a to the one measured on Si–CZ0 and the absence of this peak on SBA-15 and Si–CZ100 support this assignment. Moreover, an increase in the intensity of this peak with an increase in cerium content in the composites is found.

After exposure to NO_2, the intensity of the peaks at pK_a higher than 9 decreased, suggesting that the weakly acidic –OH groups are consumed during the reactive adsorption of NO_2. On the other hand, an increase in the intensity of the peak around 7, assigned to the Ce^{4+} cations, is revealed on the mixed oxides and Si–CZ0. In addition, this species does not appear with SBA-15 or Si–CZ100 confirming its cerium origin. This is more evidence that Ce^{3+} cations, which are susceptible to oxidation, are the active species in the reactive adsorption of NO_2. One has to remember that even though nitrates and/or nitrites can be formed, the experimental window of the pH between 3.5 and 11.5 for the potentiometric titration method excludes their identification since their pK_a are respectively –1.37 and 3.37 [48].

The surface chemistry was also investigated by thermal analysis where the decomposition/desorption of potential product of the reactive NO_2 adsorption is analyzed. Weight loss derivative curves for the initial and exhausted samples are collected in Fig. 11. The peaks at about 100 °C observed on the DTG curves before or after exposure to NO_2 are ascribed to the removal of moisture. For SBA-15 and Si–CZ0 the curves are featureless whereas for Si–CZ100 a peak at about 160 °C related to the dehydroxylation of terminal OH groups of zirconium hydroxide is revealed [46,49]. This peak is also visible on DTG curves for the mixed oxides composites. The intensity of this peak increases with the increase in the content of $Zr(OH)_4$.

After exposure to NO_2, two new broad peaks are revealed on the DTG curves for mixed oxides. The peak, which appears below 300 °C is assigned to the decomposition of nitrite species formed during the exposure to NO_2 [50,51]. The peak over 300 °C is linked to the decomposition of nitrate species also formed during the reactive adsorption [50,51]. Considering that the surface chemistry of our materials differs, some differences in the temperatures of decomposition of nitrites and nitrates are expected. It is interesting that nitrites and nitrates formed on the materials with the highest content in $Zr(OH)_4$ (Si–CZ100 and Si–CZ80) appear to be more stable (higher temperature of decomposition) than those on the other materials. Moreover, it seems that the amount of nitrates decomposed (signal higher than 300 °C) increases for the materials rich in zirconia suggesting that nitrates are preferentially formed on zirconia. On SBA-15 and Si–CZ0 the intensity of the peaks is much smaller. That intensity seems also to be independent of the NO_2 adsorption capacity. The analysis of the weight loss indicates that the decomposition of nitrite and nitrate species represents only about 22–30% of the NO_2 adsorption capacity regardless the composite used. This suggests that reduction of a part of NO_2 into N_2O

or N_2 should not be ruled out. Unfortunately, we are not able to detect them in our system.

In the case of mixed oxides it is, however, difficult to discuss the potential reactivity of the –OH groups, as it was suggested elsewhere [29], since after exposure to NO_2, the peaks ascribed to the dehydration process and the signals due to the decomposition of nitrite species are sometimes overlapped. Nevertheless, since the consumption of –OH is clearly visible in the case of Si–CZ100 it suggests that –OH groups are involved in the NO_2 adsorption mechanism.

FTIR (not shown here) analysis has been carried out to confirm the formation of nitrite and nitrates. Unfortunately, the characteristic vibrations of nitrate and nitrites species reported on ceria–zirconia mixed oxides at about 1040–1070 cm^{-1} and 1350 cm^{-1} [50] and expected on the composites, are apparently overlapped by a broad peak due to the vibration of Si–O–Si bonds at 1070 cm^{-1} and 1300 cm^{-1} [52].

Based on the characterization of the materials before and after exposure to NO_2, a mechanism of reactive adsorption is suggested, in order to elucidate the impacts of structural and chemical parameters on the NO_2 retention process at ambient temperature. Since the presence of Ce^{3+} cations, caused by the insertion of Zr^{4+}, leads to a strong enhancement of the NO_2 adsorption capacity this cations are considered as the main centers taking part in NO_2 reactive adsorption. This is also related to the high reactivity of oxygen vacancies, associated with the reduced cerium. The higher NO_2 adsorption capacities were, indeed, found on composites, which have more oxygen vacancies than pure ceria or zirconium hydroxide [11]. It is believed that an electron transfer reaction occurs between NO_2 and oxygen vacancies to form nitrite species (observed by TA analysis) as well as the re-oxidation of cerium as demonstrated by Eq. (2) [51,53].

$$V_O\text{–}Ce^{3+} + NO_{2(g)} \rightarrow Ce^{4+}{=}ONO^- \quad (2)$$

$$Ce^{4+}{=}ONO^- + NO_{2(g)} \rightarrow Ce^{4+}\text{–}NO_3{}^- + NO_{(g)} \quad (3)$$

where V_O represents an oxygen vacancy.

The oxidation of the surface after exposure to NO_2 was evidenced by potentiometric titration (Figs. 9 and 10) and the decrease in the pH of the materials (Table 1). Following the Eq. (2), the nitrite species formed may be oxidized into nitrates by NO_2 according the Eq. (3). However, the higher temperature required for the decomposition of nitrite and nitrate species observed on mixed oxides richer in $Zr(OH)_4$ during thermal analysis (Fig. 11) have to be taken into account in our discussion. Therefore the formation of bridging nitrate cannot be ruled out as described by Eq. (4).

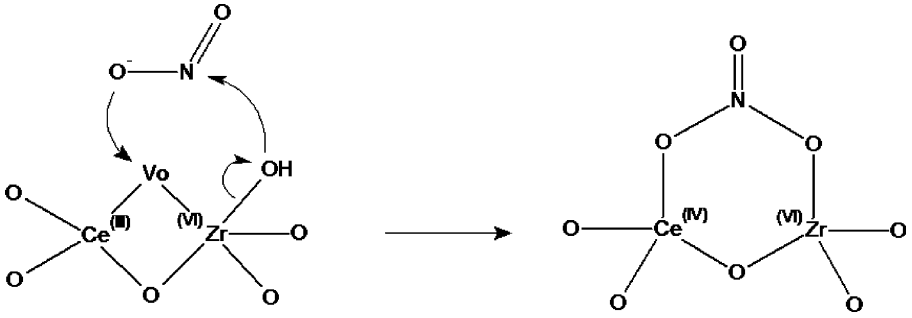

(4)

where V_O represents an oxygen vacancy.

The formation of such bridging nitrate species, which are known to be more stable in comparison with monodentate nitrates species formed according to Eqs. (2) and (3) [54], was identified based on FTIR data obtained on the $Ce_{1-x}Zr_xO_2$ samples exposed to NO_2 [29].

The reactivity of –OH groups towards NO_2 and NO at ambient temperature has also to be taken into consideration since a consumption of these groups was revealed on pK_a distributions.

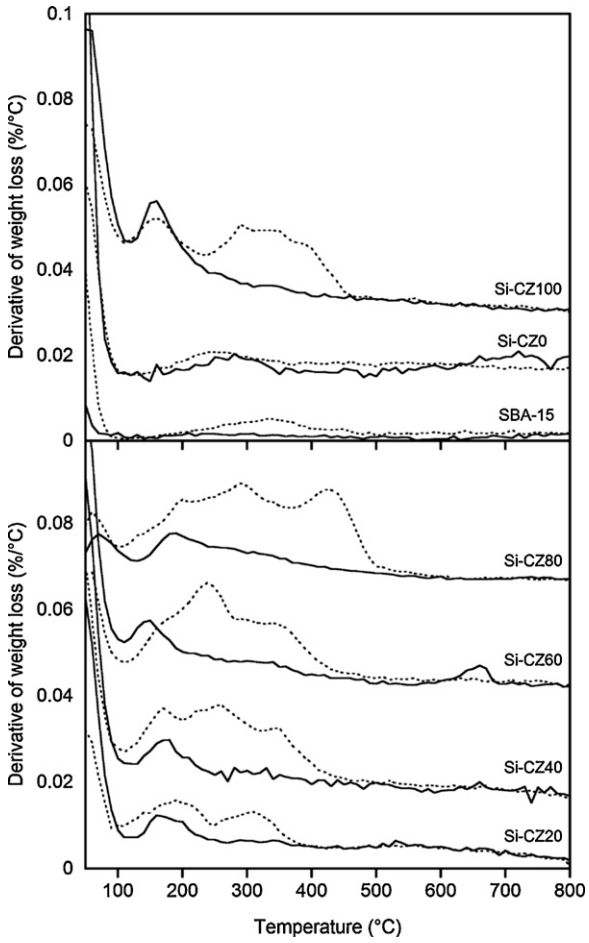

Fig. 11. Thermal analysis of DTG curves of SBA-15 Si–CZ composites before (solid) and after (dotted) exposure to NO_2.

Moreover, as shown in Fig. 1 and Table 1, the retention of NO increases with an increase in the density in hydroxyl groups originating from $Zr(OH)_4$. Thus two reactions are suggested involving –OH and NO_x [29]:

$$2Ce^{4+}\text{–}OH + NO_2 \rightarrow Ce^{4+}\text{–}NO_3{}^- + Ce^{3+}\text{–}V_O + H_2O \quad (5)$$

$$2Ce^{4+}\text{–}OH + NO \rightarrow Ce^{4+}\text{–}NO_2{}^- + Ce^{3+}\text{–}V_O + H_2O \quad (6)$$

where V_O represents an oxygen vacancy.

NO_2 or NO is expected to react with –OH leading to the formation of respectively nitrites or nitrates as well as to the reduction of ceria [55]. However, this kind of reactions is believed to occur also on terminal Zr–OH and silanol since some changes in proton binding curves and pK_a distributions were observed on SBA-15 alone and Si–CZ100. The reactivity of silanol groups is, in addition, in agreement with the change in the pore size distribution of the SBA-15 after exposure to NO_2. Thus the higher NO_2 adsorption capacities

measured on the composites materials are explained by the higher density in both oxygen vacancies, associated with Ce^{3+} cations and in –OH groups due to the insertion of Zr^{4+} cations in the fluorite structure of CeO_2.

4. Conclusions

The mixed oxides $Ce_{1-y}Zr_yO_{2-x}$ were successfully dispersed on the surface of mesoporous silica SBA-15. The new composite materials have a mesoporous structure with a 2D-hexagonal network of pores, in spite of a slight disorganization of this network due to the utilization of NaOH as precipitating agent. The decrease in the size of the pores clearly indicates that the mixed oxides are formed inside of them. This high dispersion is responsible for an enhancement in the NO_2 adsorption capacity of the composite materials in comparison with the capacities measured on mixed oxides synthesized without a mesoporous support. It is proposed that the reduction of Ce^{4+} into Ce^{3+} due to the insertion of Zr^{4+} in ceria fluorite structure is a major factor enhancing NO_2 adsorption at ambient conditions. Ce^{3+} cation is considered as the active adsorption sites of NO_2 and it contributes, by electron transfer reaction, to the formation of nitrite and nitrates species on the materials. Another important centers enhancing the retention of NO_x are also –OH groups, which take part in the oxidation process. Thus any increase in the amount of Ce^{3+} in the structure by addition of $Zr(OH)_4$ is associated with an increase in the density of –OH. High dispersion of these adsorption centers in the pore system intensifies their contact with the adsorbate and thus enhances the adsorption capacity. After exposure to NO_2 the structure remains quite stable since only a decrease of around 15% in the volume of pores was measured on Si–CZ80 after exposure to NO_2.

Acknowledgment

This study was supported by the ARO (Army Research Office) grant W911NF-10-1-0030.

References

[1] J.N. Armor, Catalytic reduction of nitrogen oxides with methane in the presence of excess oxygen: a review, Catal. Today 26 (1995) 147–158.
[2] V.I. Parvulescu, P. Grange, B. Delmon, Catalytic removal of NO, Catal. Today 46 (1998) 233–316.
[3] M.D. Fokema, J.Y. Ying, The selective catalytic reduction of nitric oxide with methane over nonzeolitic catalysts, Catal. Rev.: Sci. Eng. 43 (2001) 1–29.
[4] A. Trovarelli, Catalytic properties of ceria and CeO_2-containing materials, Catal Rev.: Sci. Eng. 38 (1996) 439–520.
[5] J. Kaspar, P. Fornasiero, M. Graziani, Use of CeO_2-based oxides in the three-way catalysis, Catal. Today 50 (1999) 285–298.
[6] G. Madia, M. Koebel, M. Elsener, A. Wokaun, Side reactions in the selective catalytic reduction of NO_x with various NO_2 fractions, Ind. Eng. Chem. Res. 41 (2002) 4008–4015.
[7] Y. Namai, K. Fukui, Y. Iwasawa, The dynamic behaviour of CH_3OH and NO_2 adsorbed on CeO_2 (1 1 1) studied by noncontact atomic force microscopy, Nanotechnology 15 (2004) S49–S54.
[8] U. Berner, K. Schierbaum, G. Jones, P. Wincott, S. Haq, G. Thornton, Ultrathin ordered CeO_2 overlayers on Pt(1 1 1): interaction with NO_2, NO, H_2O and CO, Surf. Sci. 467 (2000) 201–213.
[9] J.A. Rodriguez, T. Jirsak, S. Sambasivan, D. Fisher, A. Maiti, Chemistry of NO_2 on CeO_2 and MgO: experimental and theoretical studies on the formation of NO_3, J. Phys. Chem. 112 (2000) 9929–9939.
[10] M. Nolan, Molecular adsorption on the doped (1 1 0) ceria surface, J. Phys. Chem. C 113 (2009) 2425–2432.
[11] G. Balducci, M. Saiful Islam, J. Kaspar, P. Fornasiero, M. Graziani, Bulk reduction and oxygen migration in the ceria-based oxides, Chem. Mater. 12 (2000) 677–681.
[12] Z. Yang, T.K. Woo, K. Hermansson, Effect of Zr doping on stoichiometric and reduced ceria: a first-principles study, J. Chem. Phys. 124 (2006) 224704-1–224704-7.
[13] G. Balducci, P. Fornasiero, R. Di Monte, J. Kaspar, S. Meriani, M. Graziani, An unusual promotion of the redox behavior of CeO_2–ZrO_2 solid-solutions upon sintering at high-temperatures, Catal. Lett. 33 (1995) 193–200.
[14] L.F. de Mello, M.A.S. Baldanza, F.B. Noronha, M. Schmal, NO reduction with ethanol on MoO_3/Al_2O_3 and CeO_2-ZrO_2-supported Pd catalysts, Catal. Today 85 (2003) 3–12.
[15] R. Burch, D. Ottery, The selective reduction of nitrogen oxides by higher hydrocarbons on Pt catalysts underlean-burn conditions, Appl. Catal. B: Environ. 13 (1997) 105–111.
[16] A.B. Ross, J.M. Jones, S. Chaiklangmuang, M. Pourkashanian, A. Williams, K. Kubica, J.T. Andersson, M. Kerst, P. Danihelka, K.D. Bartle, Measurement and prediction of the emission of pollutants from the combustion of coal and biomass in a fixed bed furnace, Fuel 81 (2002) 571–582.
[17] C.T. Kresge, M.E. Leonowicz, W.J. Roth, J.C. Varfuli, J.S. Beck, Ordered mesoporous molecular-sieves synthesized by a liquid–crystal template mechanism, Nature 359 (1992) 710–712.
[18] J.S. Beck, J.C. Varfuli, W.J. Roth, M.E. Loenowicz, C.T. Kresge, K.D. Schmitt, C.T.-W. Chu, D.H. Olsen, E.W. Sheppard, S.B. McCulne, J.O. Higgins, J.L. Schlenker, A new family of mesoporous molecular-sieves prepared with liquid–crystal templates, Am. Chem. Soc. 114 (1992) 10834–10843.
[19] A. Stein, B.J. Melde, R.C. Schroden, Hybrid inorganic–organic mesoporous silicates—nanoscopic reactors coming of age, Adv. Mater. 12 (2000) 1403–1419.
[20] U. Junges, W. Jacobs, I. Voight-Martin, B. Krutzsch, F. Schueth, MCM-41 as a support for small platinum particles—a catalyst for low-temperature carbon-monoxide oxidation, J. Chem. Soc. Chem. Commun. (1995) 2283–2284.
[21] U. Junges, S. Disser, G. Schmid, F. Schuth, Ordered mesoporous materials as catalyst supports, Stud. Surf. Sci. Catal. 117 (1998) 391–398.
[22] M. Boutros, J.M. Trichard, P. Da Costa, Silver supported mesoporous SBA-15 as potential catalysts for SCR NO_x by ethanol, Appl. Catal. B: Environ. 91 (2009) 640–648.
[23] Z. Luan, E.M. Maes, P.A.W. van der Heide, D. Zhao, R.S. Czernuszewicz, L. Kevan, Incorporation of titanium into mesoporous silica molecular sieve SBA-15, Chem. Mater. 11 (1999) 3680–3686.
[24] T. Abe, Y. Tachibana, T. Uematsu, M. Iwamoto, Preparation and characterization of Fe_2O_3 nanoparticles in mesoporous silicate, J. Chem. Soc. Chem. Commun. (1995) 1617–1618.
[25] A. Patel, T.E. Rufford, V. Rudolph, Z. Zhu, Selective catalytic reduction of NO by CO over CuO supported on SBA-15: effect of CuO loading on the activity of catalysts, Catal. Today 166 (2011) 188–193.
[26] D. Zhao, J. Feng, Q. Huo, N. Melosh, G.H. Fredrickson, B.F. Chmelka, G.D. Stucky, Triblock copolymer syntheses of mesoporous silica with periodic 50 to 300 angstrom pores, Science 279 (1998) 548–552.
[27] E. Rossinyol, A. Prim, E. Pellicer, J. Rodriguez, F. Peiro, A. Cornet, J.R. Morante, B. Tian, T. Bo, D. Zhao, Mesostructured pure and copper-catalyzed tungsten oxide for NO_2 detection, Sens. Actuators B 126 (2007) 18–23.
[28] T. Wagner, T. Waitz, J. Roggenbuck, M. Froba, C.-D. Kohl, M. Tiemann, Ordered mesoporous ZnO for gas sensing, Thin Solid Films 515 (2007) 8360–8363.
[29] B. Levasseur, A.M. Ebrahim, T.J. Bandosz, Role of $Zr^{(4+)}$ cations in NO_2 adsorption on $Ce_{(1-x)}Zr_xO_2$ mixed oxides at ambient conditions, Langmuir 27 (2011) 9379–9386.
[30] C. Yu, B. Tian, J. Fan, G.D. Stucky, D. Zhao, Salt effect in the synthesis of mesoporous silica templated by non-ionic block copolymers, Chem. Commun. (2001) 2726–2727.
[31] M.M. Dubinin, Porous structure and adsorption properties of activated carbons, in: P.L. Walker (Ed.), Chemistry and Physics of Carbon, vol. 2, M. Dekker, New York, 1996, pp. 51–120.
[32] B. Smarsly, M. Thommes, P.L. Ravikocih, A.V. Neimark, Characterization of worm-like micro and mesoporous silica by small-angle scattering and high-resolution adsorption porosimetry, Adsorption 11 (2005) 653–655.
[33] J. Jagiello, Stable numerical-solution of the adsorption integral-equation using splines, Langmuir 10 (1994) 2778–2785.
[34] S. Bashkova, T.J. Bandosz, Adsorption of NO_2 at room temperature on iron-containing polymer-based porous carbons, ChemSusChem 4 (2011) 404–412.
[35] K. Kante, E. Deliyanni, T.J. Bandosz, Adsorption of NO_2 on activated carbons modified with cerium, lanthanum and sodium chlorides, J. Hazard. Mater. 165 (2008) 357–365.
[36] M. Seredych, S. Bashkova, R. Pietrzak, T.J. Bandosz, Interactions of NO_2 and NO with carbonaceous adsorbents containing silver nanoparticles, Langmuir 26 (2010) 9457–9464.
[37] R. Pietrzak, T.J. Bandosz, Activated carbons modified with sewage sludge derived phase and their application in the process of NO_2 removal, Carbon 45 (2007) 2537–22546.
[38] B. Levasseur, E. Gonzalez-Lopez, J.A. Rossin, T.J. Bandosz, Effect of reduction treatment on copper modified activated carbon on NO_x adsorption at room temperature, Langmuir 27 (2011) 5354–5365.
[39] B. Levasseur, C. Petit, T.J. Bandosz, Reactive adsorption of NO_2 on copper-based metal–organic framework and graphite oxide/metal–organic framework composites, ACS Appl. Mater. Interfaces 12 (2010) 3606–3613.
[40] M. Seredych, T.J. Bandosz, Effects of surface features on adsorption of SO_2 on graphite oxide/$Zr(OH)_4$ composites, J. Phys. Chem. C 114 (2010) 14552–14560.
[41] K. Kante, E. Deliyanni, T.J. Bandosz, Interaction of NO_2 with activated carbons modified with cerium, lanthanum and sodium chlorides, J. Hazard. Mater. 165 (2009) 704–713.
[42] S. Bashkova, T.J. Bandosz, The effects of urea modification and heat treatment on the process of NO_2 removal by wood-based activated carbon, J. Colloid Interface Sci. 333 (2009) 97–103.
[43] L. Bergström, E. Bostedt, Surface-chemistry of silicon-nitride powders-electrokinetic behavior and ESCA studies, Colloides Surf. 49 (1990) 183–197.

[44] J.A. Tossell, N. Sahai, Calculating the acidity of silanols and related oxyacids in aqueous solution, Geochim. Cosmochim. Acta 64 (2000) 4097–4113.
[45] A.M. Shaw, T.E. Hannon, F. Li, R.N. Zare, Adsorption of crystal violet to the silica–water interface monitored by evanescent wave cavity ring-down spectroscopy, J. Phys. Chem. B 107 (2003) 7070–7075.
[46] P.W. Schindler, W. Stumm, The surface chemistry of oxides, hydroxides and oxide minerals, in: W. Stumm (Ed.), Aquatic Surface Chemistry, Wiley, New York, 1987, pp. 83–110.
[47] Toxicological review of cerium oxide and cerium compounds, EPA/635/R-08/002F, U.S. Environmental Protection Agency, Washington DC, 2009.
[48] R.C. Weast, M.J. Astle, Chemical general, in: Handbook of Chemistry and Physics, CRC Press, Boca Raton, Fl, 1982, p. B-99.
[49] T.J. Bandosz, J. Jagiello, J.A. Schwarz, Surface-acidity of pillared taeniolites in terms of their proton affinity distributions, J. Phys. Chem. 99 (1995) 13522–13527.
[50] B. Azambre, I. Atribak, A. Bueno-Lopez, A. Garcia-Garcia, Probing the surface of ceria–zirconia catalysts using NO_x adsorption/desorption: a first step toward the investigation of the crystallite heterogeneity, J. Phys. Chem. C 114 (2010) 13300–13312.
[51] N. Nolan, S.C. Parker, G.W. Watson, Reduction of NO_2 on ceria surfaces, J. Phys. Chem. B 110 (2006) 2256–2262.
[52] Y. Li, B. Yan, J.L. Liu, Luminescent organic–inorganic hybrids of functionalized mesoporous silica SBA-15 by thio-slicylidene Schiff base, Nanoscale Res. Lett. 5 (2010) 797–804.
[53] G.Y. Guo, Y.L. Chen, W.J. Ying, Thermal, spectroscopic and X-ray diffractional analyses of zirconium hydroxides precipitated at low pH values, Mater. Chem. Phys. 84 (2004) 308–314.
[54] X. Zhang, H. He, H. Gao, Y. Yu, Experimental and theoretical studies of surface nitrate species on Ag/Al2O3 using DRIFTS and DFT, Spectrochim. Acta Part A 71 (2008) 1446–1451.
[55] I. Atribak, B. Azambre, A. Bueno Lopez, A. Garcia-Garcia, Effect of NO_x adsorption/desorption over ceria-zircconia catalysts on the catalytic combustion of model soot, Appl. Catal. B: Environ. 92 (2009) 126–137.